The formation of ordered clusters in Ti-7Al and Ti-6Al-4V

A. Radecka[a,f], P.A.J. Bagot[d], T.L. Martin[d], J. Coakley[b,c], V.A. Vorontsov[a], M.P. Moody[d], H. Ishii[e], D. Rugg[f], D. Dye[a]

[a]*Department of Materials, Royal School of Mines, Imperial College London, Prince Consort Road, London, SW7 2BP, UK*
[b]*Department of Materials Science and Metallurgy, University of Cambridge, Cambridge CB3 OF3, UK*
[c]*Department of Materials Science and Engineering, Northwestern University, 2220 Campus Drive, Evanston, IL 60208-3108, USA*
[d]*Department of Materials, University of Oxford, Oxford OX1 3PH, UK*
[e]*Hawaii Institute of Geophysics and Planetology, University of Hawaii, Manoa HI 96822, USA*
[f]*Rolls Royce, Elton Road, Derby, DE24 8BJ, UK*

Abstract

Ti-Al alloys can suffer from a chemical decomposition on ageing around 500 °C or on air cooling. At long ageing times this results in the formation of α_2 (Ti_3Al) precipitates. At reduced times or elevated temperatures, diffuse electron or neutron diffraction peaks can be observed, which has been termed 'short range ordering' (SRO). Here, we present correlative transmission electron microscopy (TEM) and atom probe tomography (APT) results showing that the reaction proceeds through the formation of ordered Al-rich precipitate clusters. Notably, Al-Al clustering could be observed well before the appearance of distinct precipitates in the TEM. In addition, the V-containing α phase of Ti-6Al-4V formed ordered clusters much faster than in binary Ti-7Al. This implies that the ternary addition of β stabilisers exacerbates the problem of α_2 precipitate formation in commercial dual phase titanium alloys.

Keywords: Titanium alloys, atom probe tomography (APT), ordering, transmission electron microscopy (TEM)

1. Introduction

Titanium alloys are widely utilised in aero-engine applications for critical rotating parts, with the majority of the commonly used α+β alloys possessing an Al concentration between 6 and 8 wt.% [1, 2, 3]. Ti-6Al-4V (wt.%) is an $\alpha+\beta$ alloy that offers a combination of good specific fatigue strength and corrosion resistance, and is therefore commonly used in aerospace applications [2]. The binary α-Ti alloy Ti-7Al (12Al at.%) is frequently used [4, 5] as a model alloy to represent the α phase of Ti-6Al-4V. Thus there is an implicit assumption that the α phase is totally depleted in V, which is a β-stabiliser.

Cold dwell fatigue is a phenomenon where holding periods at load of the order of 2 minutes result in large ($10\times$) reductions in cyclic life. This is of concern to jet engine manufacturers for components such as Ti-6Al-4V fan discs.

*Corresponding Author. Email david.dye@imperial.ac.uk, Tel: +44 797 707 6141 (no fax).

In Al-containing alloys, ordering of the α-phase, observed as diffuse spots corresponding to the Ti_3Al structure in selected area transmission electron diffraction (SAD) patterns, has been frequently found to co-occur with poor dwell fatigue performance [6, 7]. At long ageing times at low temperatures around 500 °C, these diffuse spots can eventually become identifiable single crystal electron diffraction spots that permit the imaging of nanoscale α_2 precipitates [8]. The effect of heat treatment times and temperatures on α_2 size for Ti-Al alloys with different Al concentrations has been studied since the late 1960s [8, 9, 10, 11, 12], but is still not well understood.

Ordering and spinodal decomposition result in a change in the dislocation behaviour, so the presence of the α_2 phase may be suggested based on the observed dislocation network. Short, straight segments of prism $[11\bar{2}0]\{10\bar{1}0\}$ dislocations are observed to travel in pairs, as is required to avoid creating stacking faults in the α_2 phase [13, 5, 11]. Such changes are observed even where imaging of the α_2 phase is impossible, and also in samples that have been subjected to hydrogen-related hot salt stress corrosion cracking [10]. Moreover, planar slip was reported to occur [14] in alloys which were aged at 500 °C, with the slip line distribution becoming coarser in alloys with higher oxygen content. Similar results were previously observed by Williams et al. [13, 15] in Ti-10Al wt.% (16Al at.%). It was suggested that the degree of order can influence the the slip nature (planar or wavy), and the slip distribution (coarse or fine). The appearance of the very coarse, planar slip was explained by the fact that dislocations cut the α_2 particles.

The quantification of this ordering and spinodal decomposition phenomenon for air cooled samples or those aged at 625 °C has remained very difficult [16, 17]. In principle, the difference between the Ti_3Al and hexagonal close packed (HCP) α-Ti phases is twofold; (i) α-Ti has a solubility for Al of only $\sim$10 at.%, and (ii) in Ti_3Al, no Al-Al bonds exist. Therefore, it might be possible for ordering of α-Ti to occur without long-scale chemical decomposition (only ii), or that a conventional chemical decomposition must first occur that enables the formation of ordered Ti_3Al precipitates. Superlattice spots have been observed [9, 11] in transmission electron microscopy (TEM). Furthermore, Neeraj et al. [18, 19] observed broad diffuse scattering peaks in neutron diffraction in Ti-6Al wt.% (10Al at.%), which have also been observed in Ti-7Al wt.% (12Al at.%) by Fitzner et al. [20]. Both Neeraj [19] and Brandes in Ti-7Al wt.% (12Al at.%) [5] observed diffuse spots in TEM, which could be suppressed by water quenching to provide a fully disordered α-Ti structure. More recently, ordering in the α phase of Ti-6Al-4V has been observed by Wu et al. [21] at relatively short ageing times of 35 days at 500 °C. In addition, Liew et al. [17] studied Ti-9Al wt.% (15Al at.%) by field ion microscopy (FIM) after 500 hours ageing at 650 °C and 750 °C, where ordering could be observed in the TEM but compositional variations could not. Therefore, the problem of quantifying this precipitation phenomenon has remained strongly intractable to analysis, by 1998-era atom probe tomography instruments (APT) [22, 23, 24, 25], by TEM and by neutron diffraction.

Recent advances APT enable this question to be revisited, and this is the topic of the present paper. APT is accompanied by conventional TEM using high dynamic range diffraction pattern characterisation. It is found that precipitation appears to occur much faster, and more strongly, in α-Ti which is alloyed, very slightly, with V in Ti-6Al-4V than in the pure binary Ti-Al. This is compared to results for Ti-Al-V [21], Ti-Al-

Mo [26] and Ti-Al-Zr [27] alloys, where similar ternary alloying effects are observed.

2. Experimental Description

2.1. Material preparation

An ingot of nominal composition Ti-7Al wt.% (12Al at.%) Al was prepared by vacuum arc melting and hot rolled to 13×13 mm square bar at Timet Witton, Birmingham, UK. Commercial purity Ti sponge was used to obtain industrially representative levels of Fe and Si, and an O content of 1800 ppmw. The ingot was first homogenised at 1125 °C and then β forged. β phase profile rolling followed by $\alpha+\beta$ phase profile rolling was performed at 1125°C and 800°C respectively in order to reduce the ingot to the final dimensions. Figure 1 contains images of the ingot preparation.

[Figure 1 about here.]

The rolled bar was then encapsulated in quartz under low pressure Ar and recrystallised at 1125 °C for 60 min. An equiaxed microstructure with a homogenous grain size distribution of $\sim 30\,\mu$m was obtained. Electron backscatter diffraction (EBSD) analyses of the samples were obtained using a Zeiss Auriga scanning electron microscope (SEM). The final microstructure and texture pole figures are provided in Figure 2(a-b). It is evident that a strong $\{11\bar{2}0\}$ rolling texture was produced.

[Figure 2 about here.]

A plate of Ti-6Al-4V of measured composition 6.49Al, 4.04V, 0.22O, 0.16Fe wt.% (11.0Al, 3.6V, 0.6O, 0.1Fe at.%) manufactured by Timet was supplied by Rolls-Royce plc (heat HUB2428), in a near-equiaxed creep flattened and slow cooled in induction furnace condition. A representative SEM micrograph is shown in Figure 2(c); the material is further characterised in [28].

According to the Ti-Al phase diagram experimentally determined by Namboodhiri [29], there is a short-range-ordering (SRO) region at an ageing temperature of ~ 600 °C for Ti-Al alloys with concentrations around 6-7 wt.%. The ordering state of Ti-7Al was manipulated by employing different heat-treatment routes to produce five conditions of interest. The heat treatments were as follows: 920 °C for 10 min, followed by (i) ice water quenching (IWQ), (ii) air cooling (AC), (iii) AC and then ageing at 625 °C for 14 days (625/14), (iv) AC and then ageing at 550 °C for 28 days (550/28), and finally (v) AC and then ageing at 550 °C for 84 days (550/84). These five conditions were intended to produce progressively greater amounts of ordering. Samples of Ti-6Al-4V were heat treated as follows: 930 °C , followed by (i) slow cooling (SC), (ii) SC and then ageing at 625 °C for 14 days (625/14), (iii) SC and then ageing at 550 °C for 28 days (550/28). The five heat-treatments of Ti-7Al and three heat-treatments of Ti-6Al-4V used in this study are presented in Table 1.

2.2. Transmission electron microscopy

Specimens for TEM were produced by spark eroding thin discs 3 mm in diameter, which were then ground to a thickness of ~ 0.15 mm and thinned to perforation with a Tenupol-5 twin-jet electropolisher using 3% perchloric acid ($HClO_4$), 40% butan-1-ol ($C_4H_{10}O$) and 57% methanol (CH_3OH) at -40 °C with an applied voltage between 20 and 25 V. Cooling the electrolyte minimises the amount of adsorbed hydrogen and results in more controlled polishing [30].

Samples from primary α grains in the Ti-6Al-4V alloy were produced by in-situ lift out in a dual beam focused ion beam/scanning electron microscope (FIB/SEM) [31, 32].

Transmission electron microscopy was performed using a (i) JEOL 2000FX 200kV TEM equipped with an Oxford Instruments ultra-thin window energy dispersive X-ray spectrometer (EDS), (ii) JEOL 2100F 200kV TEM/STEM equipped with EDS (XMax, Oxford Instruments) and EELS (Gatan, Quantum GIF with 0.8 eV energy resolution) and an (iii) FEI Titan 80-300 keV monochromated and dual Cs-corrected TEM/STEM.

2.3. Atom probe tomography

APT samples were prepared by the FIB lift-out method using a FEI Helios NanoLab 600 DualBeam system equipped with an Omniprobe^{TM}. A detailed description of the lift-out and tip sharpening procedure can be found in references [33, 34, 35, 36]. Atom probe experiments were performed in the voltage-pulsing mode using a CAMECA LEAP 3000X HR and a LEAP 4000X Si. The stage temperature and the voltage pulse fraction were set to 55K and 15%, respectively. After data collection, the atom maps from the runs were reconstructed utilising IVAS^{TM} data analysis software [37].

3. Results and discussion

3.1. TEM investigation

The APT investigations were complemented by dark field TEM imaging based on electron diffraction experiments carried out to identify and visualise any precipitates or ordered structures present.

[Figure 3 about here.]

Prior experimental work on Ti-Al alloys showed that ordering could develop in alloys that had been aged or have been used in service at relatively low temperatures of around 500 °C [18, 6]. A variety of methods have been used to investigate this phenomenon. Some contention has arisen around the $\alpha \backslash (\alpha + \alpha_2)$ phase boundary due to the fact that the ordered regions are indirectly visible only using high resolution techniques after prolonged heat treatments [18, 6, 17]. The majority of publications on SRO have been based on TEM studies, particularly the analysis of SAD patterns. It was previously reported that Ti_3Al precipitates could be easily identified, as these produce superlattice reflections in SAD patterns [39]. Superlattice reflections occur symmetrically between the reflections from the disordered matrix along certain directions. This phenomenon is due to the fact that the lattice parameter of α_2 is approximately twice

that of α. However, many studies [10, 11, 12, 17, 18] have shown the superlattice reflections in diffraction patterns of α and near-α titanium alloys after ageing, but very often it has not been possible to image ordered regions in dark field TEM. This has been explained by suggesting that the ordered regions were too small to be resolved. Although more work needs to be done to obtain conclusive evidence of the ordered structure, it seems to be reasonable to attribute the extra electron diffraction spots to the formation of ordered structures in the Ti-Al system.

[Figure 4 about here.]

In the IWQ and AC samples, only fundamental reflections from the matrix are evident in the SAD patterns, Figure 3(a-b). In contrast, the extra diffraction spots seen in Figures 3(c-d) arise from the ordered phase. After heat treatment for 84 days at 550 °C, the superlattice reflections were strong enough to allow imaging in dark field of the ordered regions, Figure 4. From the samples which were aged for shorter times, it was not possible to obtain dark field images of precipitates.

The intensity of superlattice reflections depends on the sample thickness, holder tilt, and time of exposure. As a result, various zone axes and long exposure times were used to study ordering through the analysis of the diffraction patterns. Table 1 qualitatively compares the intensity of the visible superlattice reflections for different heat treatment conditions. The charge-coupled devices (CCD) commonly used in modern TEM cameras can be damaged by prolonged exposures, and so a JEOL 2100F TEM/STEM electron microscope was used, equipped with a camera and photographic film, allowing long exposure times. In the Ti-7Al (IWQ and AC) samples, even after a long exposure times, only reflections from the matrix were visible on the negatives. Reflections described as very, very weak were only seen on the negative when overexposed. In Ti-7Al samples 550/28 and 625/14, although the superlattice spots were clearly dimly visible, it was not possible to image precipitates of the α_2 phase in dark field mode, even with prolonged exposure times.

[Table 1 about here.]

High angle annular dark field (HAADF) scanning transmission electron microscopy (STEM) imaging was carried out to try to visualise any compositional changes due to Ti_3Al ordering in Ti-7Al and Ti-6Al-4V (wt.%), in all conditions. No obvious contrast differences were observed on length scales from 1-500 nm that could be attributed to Ti_3Al ordering. EDX, carried out on a JEOL 2100F TEM/STEM operating at 200kV and fitted with an Oxford Instruments XMax detector, confirmed that 6-7 wt.% Al was present in the Ti samples, but it was not possible to detect any local compositional variations.

According to Blackburn [10], α_2 particles observed in Ti-8Al wt.% (13Al at.%) are spherical in shape initially and maintain this geometry up to around 50 nm, finally elongating to form ellipsoids with the major axis lying along the [0001] direction. Blackburn observed rapid growth of the α_2 phase once it was formed, however, the growth rate decreased at long ageing times. Similar results were later obtained by Namboodhiri et al. [11] in alloys containing 8.5 and 16.5 wt.% Al (13.8 and 23.8Al at.%). They

observed a change in morphology from an irregular shape to an elliptical one with a diameter of 10 nm. Our own observations are consistent with these results. In the Ti-7Al alloy aged for 84 days at 550 °C, dark-field microscopy using a superlattice reflection revealed features 20 × 150 nm in size with an elliptical morphology. These can be clearly seen in Figure 4.

Electron diffraction experiments were also carried out on the Ti-6Al-4V samples. The α phase in Ti-6Al-4V was found, using EDX in the SEM, to have the approximate composition of Ti-7.6Al-2.3V wt.% (12.8Al-2.0V at.%) , with the remaining vanadium mostly rejected to the β, as seen using EDX in the SEM. Diffraction patterns taken from the α phase of the SC sample contained additional spots to the fundamental reflections, Figure 5a. These additional weak reflections in the recorded SAD patterns imply that ordered domains are present. Figure 5(b-c) presents electron diffraction patterns taken from Ti-6Al-4V samples which were aged for 14 days at 625 °C and for 28 days at 550 °C, respectively. Clearly visible superlattice reflections suggest that such ordered domains have an α_2 hexagonal $D0_{19}$ crystal structure.

[Figure 5 about here.]

The results of the SAD pattern observations in the present specimens of Ti-6Al-4V aged at temperatures between 550 and 625 °C, suggest that the ordering in this alloy is faster than in the binary Ti-7Al alloys under similar conditions. Thus, while it is confirmed that ordering occurs in Ti-Al alloys with Al concentrations of around 6 wt.% (10 at.%), then moreover it appears that V additions to α Ti, even at quite small concentrations, result in faster α_2 formation.

The Ti-6Al-4V sample aged at 550 °C for 28 days was also examined by HRTEM in the JEOL 2100F, Figure 6. Spatial variations in the overall intensity of the atomic columns in high resolution imaging could be observed. When fast Fourier transforms (FFT) were taken of different subregions of the image, then in some of these regions (2 and 4), faint evidence of an α_2 spot could be observed. Line profile analyses between the $\{0\bar{1}1\bar{1}\}$ and $\{000\bar{1}\}$ spots are shown in Figure 7, and also indicate the presence of a peak corresponding to the α_2 in subregions 2 and 4.

[Figure 6 about here.]

[Figure 7 about here.]

A dark field image taken using the superlattice spot from this sample in a image aberration-corrected Titan TEM is shown in Figure 8, which also shows spatial variations in intensity. Therefore, there is strong evidence for local variations in the extent of ordering, on the scale of 15-300 nm.

[Figure 8 about here.]

The TEM studies in Ti-6Al-4V of Wu et al. [21] found weak superlattice maxima in doubly exposed diffraction patterns taken from a sample slowly cooled from 930 °C. However, it was not possible to obtain dark field images of precipitates from these reflections as they were very weak. Furthermore, in samples aged for 35 d at 500 °C,

the development of α_2 precipitates within the α phase was observed. It was reported that these precipitates possessed a composition of Ti_3Al with a diameter between 5 and 10 nm. Wu et al. [21] also presented APT studies illustrating Al-rich clusters corresponding to the Ti_3Al phase observed in the electron diffraction patterns. In the centre of the precipitates, the Al concentration was reported to be 20 at.% and the V concentration was approximately 2 at.%. The latter figure was much greater than the expected value, and it was speculated that slower diffusion of V contributes to this; the fact that diffusion would have to take place through an ordered α_2 structure would further decrease the rate of diffusion. However, no experimental work was reported to confirm this hypothesis.

In summary, electron diffraction shows that ordered α_2 hexagonal $D0_{19}$ forms more rapidly in Ti-6Al-4V than in Ti-7Al. Thus, V in the α phase increases the precipitation kinetics. Dark field imaging of Ti-7Al shows aligned α_2 precipitates of elliptical morphology, 20×150 nm in size. This is in agreement with Blackburn and Namboodhiri et al. [10, 11]. For Ti-6Al-4V 550/28, FFT analysis of HRTEM micrographs combined with dark field imaging from an aberration corrected Titan TEM provide strong evidence for local variation in the extent of ordering through the microstructure.

3.2. APT studies

Even though many cluster identification algorithms have been developed, identifying the early formation of such features and determining their composition from APT reconstructed volumes may be non-trivial, particularly for alloys containing increasing amounts of solute [25]. A description of SRO can be attempted in terms of the nearest neighbour (NN) distributions. One technique commonly used to investigate this problem within an APT reconstruction is applying a k^{th}-order nearest neighbour (kNN) analysis, which is particularly useful when looking for subtle clustering effects in alloys containing a significant amount of solute [22, 23, 24]. Other approaches are also available [38]. For very dilute alloys, the average 1NN distance between solutes in a cluster compared to solutes in the matrix will be significant, and therefore sufficient to isolate any clusters. However, for the present alloy, the 1NN distance between Al atoms in a cluster will be very similar to that in the matrix. (i.e. there is always another Al atom very close by). Only if we look at higher order nearest neighbours, such as 10NN, 20NN, 50NN and 100NN do we start to see clear deviations from a random distribution. On the other hand, it should be recalled that if k is small it is more sensitive to very small fluctuations, for example clusters that may only consist of 5 solute atoms. However small k analyses may be subject to significant random fluctuations. Larger k values are more resistant to random fluctuations, but they also reduce the sensitivity (i.e. the size of clusters that can be identified) [24]. In the present case the bulk concentration of Al requires the use of a large k. The above discussion justifies the variety of different kNN chosen to highlight the distribution of distances separating each Al atom and its k^{th} nearest neighbour Al atoms, Figure 9. In each case, a randomised data set is used as a comparator, (R).

[Table 2 about here.]

[Figure 9 about here.]

Analysing the 10NN distribution of the Ti-6Al-4V 550/28 sample, Figure 9, it can be seen that the experimental data and corresponding random distribution closely coincide. The broadening of the peaks for 50NN, 70NN and 100NN in comparison to their respective random distributions indicates a non-random distribution of Al atoms in the experimental data. The relatively greater counts at lower separations indicate a significant number of Al atoms distributed closer together than would be randomly expected, indicative of solute clustering [24]. In Figure 10(a-b), the data (D) and randomised (R) distributions are visualised, with blue points marking Al atoms that have Al neighbours within 1.12 nm. Visually, nearest-neighbour ordered regions on the order of 5 nm in size can be observed quite clearly in the data, which are barely present in the randomised data. The features appearing in the complementary random distribution are indicative of trajectory aberrations in the experiment leading to high density regions at the top of the reconstruction. However, since these regions are incorporated in both the experimental and randomised 50NN distributions they will not affect the statistical comparison between the two distributions.

[Figure 10 about here.]

These isolated Al-rich clusters were demarcated using a 20 at.% Al isosurface, and an Al concentration profile averaged across five similar clusters was generated. This suggests that these clusters have an Al content in excess of 20 at.%, Figure 10(c). This whole analysis was repeated on a duplicate sample of 550/28 Ti-6Al-4V, with the same results obtained. The 550/28 and 625/14 Ti-7Al samples were also examined, and no such clusters were found. In the Ti-6Al-4V 625/14 sample, some very tentative evidence for clustering could be observed in the 50NN distribution, but not at a level that was distinguishable from the randomised distribution.

In Ti-7Al the composition profiles showed only very marginal statistical fluctuations for the 50NN, 70NN and 100NN distributions in comparison to the randomised datasets. Although the TEM images show superlattice reflections, there was no evidence of Ti_3Al precipitates from the APT experiments. The overall compositions of Ti-7Al needles examined using the LEAP 3000X HR after different heat treatments are shown in Table 2. It is significant that the Al concentration in a sample which was aged for 84 days at 550 °C dropped to 4 wt.%. It is suggested that in this sample, the missing Al content was located in α_2 precipitates in regions not contained within the atom probe analysis volume. From the TEM image, Figure 4, it can be clearly seen that the spacing between individual ordered regions is very large compared to the very small analysis volumes of APT samples. Thus it is possible that APT needles were lifted out between α_2 precipitates.

In summary, a nearest neighbour analysis clearly illustrates Al clusters in Ti-6Al-4V 550/28. Based on the extensive TEM study presented, these clusters correspond to ordered α_2 precipitates. There is tentative evidence of similar clustering in Ti-6Al-4V 625/14, and no evidence of clustering in the Ti-7Al alloys. Thus there is agreement between APT and TEM, that V in the α phase increases the precipitation rate of α_2.

3.3. Discussion

Many aluminium-containing titanium alloys are used at elevated temperatures up to 500 °C, for example in aero engine compressors. In such components, dwell fatigue

can be of concern and is associated with the localisation of deformation due to the formation of $\langle a \rangle$-type dislocation ribbons in α-Ti that shows evidence of so-called short range ordering (SRO). In fact, almost all commercial titanium alloys contain α phase with Al contents high enough to place them within the $\alpha + \alpha_2$ phase region originally identified by Namboodhiri et al. [11]. However, a clear, universal definition of what is meant by SRO has been lacking. Clearly, long range ordering is observed, as corresponding diffraction peaks in electron diffraction. The large breadth and low intensity of these diffraction peaks equally clearly indicate that ordering is incomplete. The APT analysis performed here suggests that such precipitates are clusters with an Al content in excess of 20 at.%.

It is also interesting that the appearance of electron diffraction peaks was much clearer, and occurred after less ageing, in Ti-6Al-4V than in the Ti-Al binary alloy, even for quite similar α phase Al contents. This suggests that in the ternary alloy, the ~ 2 at.% V present in the α plays an important role in promoting cluster formation. This indicates that V perhaps lowers the energy of formation for the α_2 phase and/or raises the diffusivity of Al in α-Ti, e.g. by promoting vacancy formation. This is consistent with the hypothesis presented by Ramachandra [40].

Liew et al. [17, 12] have previously suggested that the formation of Al-rich clusters proceeds via a spinodal decomposition mechanism. In a spinodal, the compositional waves first form and then increases in amplitude until the stoichiometric phase compositions are formed. This is distinct from the case of, e.g. Ni_3Al, where only fully stoichiometric, ordered precipitates are observed [41]. The present work supports this hypothesis.

4. Conclusions

The formation of α_2-Ti_3Al related structures in Al-containing α Ti has been investigated during low temperature ageing from the disordered state. The following conclusions can be drawn:

1. TEM studies on Ti-7Al showed no evidence of chemical ordering in the IWQ and AC samples. Ordering, observed through the diffuse superlattice reflections in the selected area diffraction patterns, was found in samples which were annealed between at 550 °C and 625 °C for times up to 84 days.
2. After heat treatment of Ti-7Al for 84 days at 550 °C, the superlattice reflections were strong enough to allow imaging of the ordered regions using TEM. At shorter ageing times it was not possible to obtain dark field images of precipitates. The same experiment was repeated on Ti-6Al-4V (slow cooled, 550/28,625/14), and in α grains of the sample aged for 28 days at 550 °C, ordered and disordered regions were observed to co-exist.
3. A $k = 50$ nearest neighbour analysis of APT data from Ti-6Al-4V in the 550/28 condition showed that distinct Al rich regions could be observed, with an Al concentration greater than 20 at.%. Such clusters could not be observed in the Ti-7Al samples or in Ti-6Al-4V aged for lower times.
4. In the light of the present work and earlier investigations on Ti_3Al precipitation in Ti-Al alloys [40, 26, 42, 4, 43, 21, 27, 41] it is evident that ordering can occur in titanium

alloys containing more then 6 wt.% Al along with Zr, Si, Mo, or V after shorter ageing times than in the binary Ti-Al alloys.

Finally, APT was shown to be an excellent complementary method to electron diffraction studies and imaging by TEM for the study of ordering in Ti alloys.

Acknowledgements

This research was supported by a Rolls-Royce plc – EPSRC CASE studentship. Material for the study was provided by Timet. Helpful discussions with Prof. T.C Lindley, Prof. G.D.W. Smith, Prof. M.H. Loretto and Prof. I.P. Jones are gratefully acknowledged. Experimental assistance was generously provided by Prof. J.P. Bradley, Dr K.M. Rahman, Dr C. McGilvery, Dr M. Ardakani and Dr D. Isheim. VV and JC would like to acknowledge support from an EPSRC doctoral prize fellowship, EU Marie Curie fellowship respectively. DD was supported by EPSRC grants EP/K034332/1 and EP/H004882/1.

References

[1] R. Boyer, Attributes, characteristics, and applications of titanium and its alloys, JOM 62 (2010) 21–24.

[2] D. Banerjee, J. Williams, Perspectives on titanium science and technology, Acta Materialia 61 (2013) 844–879.

[3] G. Lütjering, J. Williams, Titanium, Springer, 2003.

[4] T. Neeraj, Low temperature creep of titanium alloys: Microstructure, deformation mechanisms and modeling, Ph.D. thesis, The Ohio State University, 2000.

[5] M. Brandes, Creep, fatigue and deformation of α and α-β titanium alloys at ambient temperature, Ph.D. thesis, The Ohio State University, 2008.

[6] T. Neeraj, D. Hou, G. Daehn, M. Mills, Phenomenological and microstructural analysis of room temperature creep in titanium alloys, Acta Materialia 48 (2000) 1225–1238.

[7] C. Leyens, M. Peters, Titanium and titanium alloys, John Wiley and Sons, 2003.

[8] G. Lütjering, S. Weissman, Mechanical properties of age-hardened titanium-aluminum alloys, Acta Metallurgica 18 (1970) 785–795.

[9] M. Blackburn, J. Williams, Metallurgical aspects of the stress corrosion cracking of titanium alloys, Proceedings of conference on fundamental aspects of stress corrosion cracking (1969) 620–637.

[10] M. Blackburn, The ordering transformation in titanium : aluminium alloys containing up to 25 at. pct. Al, Transactions of the Metallurgical Society of AIME 239 (1967) 1200–1208.

[11] T. Namboodhiri, C. McMahon, H. Herman, Decomposition of the α-phase in titanium-rich Ti-Al alloys, Metallurgical Transactions 4 (1973) 1323–1331.

[12] H. Liew, Short range order and phase separation in Ti-Al alloys, Ph.D. thesis, University of Oxford, 1999.

[13] J. Williams, A. Thompson, R. Baggerly, Accurate description of slip character, Scripta Metallurgica 8 (1974) 625–630.

[14] G. T. Gray III, G. Luetjering, J. Williams, The influence of oxygen on the structure, fracture, and fatigue crack propagation behavior of Ti-8.6 wt. pct. Al, Metallurgical Transactions A 21 (1990) 95–105.

[15] J. Williams, A. Sommer, P. Tung, The influence of oxygen concentration on the internal stress and dislocation arrangements in α titanium, Metallurgical Transactions 3 (1972) 2979–2984.

[16] H. Liew, G. Smith, A. Cerezo, D. Larson, Experimental studies of the phase separation mechanism in Ti-15 at.%Al, Materials Science and Engineering A 270 (1998) 9–13.

[17] H. Wood, G. Smith, A. Cerezo, Short range order and phase separation in Ti-Al alloys, Materials Science and Engineering A 250 (1998) 83–87.

[18] T. Neeraj, M. Mills, Short-range order (SRO) and its effect on the primary creep behavior of a Ti-6 wt.%Al alloy, Materials Science and Engineering A 319-321 (2001) 415–419.

[19] N. Thirumalai, Low temperature creep of titanium alloys: Microstructure, deformation mechanisms and modeling, Ph.D. thesis, The Ohio State University, 2000.

[20] A. Fitzner, D. Prakash, J. da Fonseca, M. Thomas, S.-Y. Zhang, J. Kelleher, P. Manuel, M. Preuss, Understanding the effect of aluminium on twin activity in binary alpha-titanium, Acta Materialia 103 (2015) 342–351.

[21] Z. Wu, C. Qiu, V. Venkatesh, H. Fraser, R. Williams, G. Viswanathan, M. Thomas, S. Nag, R. Banerjee, M. Loretto, The influence of precipitation of α_2 on properties and microstructure in TIMETAL 6-4, Metallurgical and Materials Transactions A 44 (2013) 1706–1713.

[22] D. Vaumousse, A. Cerezo, P. Warren, A procedure for quantification of precipitate microstructures from three-dimensional atom probe data, Ultramicroscopy 95 (2003) 215–221.

[23] L. Stephenson, M. M. P. Liddicoat, S. Ringer, New techniques for the analysis of fine-scaled clustering phenomena within atom probe tomography (APT) data, Microscopy and Microanalysis 13 (2007) 448–463.

[24] B. Gault, M. Moody, J. M. Cairney, S. Ringer, Atom probe microscopy, Springer, 2006.

[25] D. Larson, T. Prosa, R. Ulfig, B. Geiser, T. Kelly, Local electrode atom probe tomography. A User's Guide, Springer, 2013.

[26] C. Ramachandra, V. Singh, Precipitation of the ordered Ti_3Al phase in alloy Ti-6.3Al-2Zr-3.3Mo-O.3OSi, Scripta Metallurgica 20 (1986) 509–512.

[27] Y. Imbert, Creep resistance and embrittlement of a Ti-6%Al-5%Zr-1%W-0.4% Si alloy, Journal of the Less-Common Metals 37 (1974) 71–89.

[28] P. O. Tympel, T. C. Lindley, E. A. Saunders, M. Dixon, D. Dye, Influence of complex LCF and dwell load regimes on fatigue of Ti-6Al-4V, Acta Materialia 103 (2016) 77–88.

[29] T. Namboodhiri, On the Ti-Al phase diagram, Materials Science and Engineering 57 (1983) 21–22.

[30] D. Williams, C. Carter, Transmission electron microscopy, 2nd ed., Springer, 2009.

[31] J. Mayer, L. Giannuzzi, T. Kamino, J. Michael, TEM sample preparation and FIB-induced damage, MRS Bulletin 32 (2007) 400–4007.

[32] D. S. Rao, K. Muraleedharan, C. Humphreys, Microscopy: science, technology, applications and education. TEM specimen preparation techniques, volume 2, Formatex Research Center, 2010.

[33] M. Miller, Atom probe tomography: Analysis at the atomic level, Kluwer Academic/Plenum New York, 2000.

[34] K. Thompson, D. Lawrence, D. Larson, J. Olson, T. Kelly, B. Gorman, In situ site-specific specimen preparation for atom probe tomography, Ultramicroscopy 107 (2007) 131–139.

[35] K. Thompson, B. Gorman, D. Larson, B. van Leer, L. Hong, Minimization of Ga induced FIB damage using low energy clean-up, Microscopy and Microanalysis 12 (2006) 1736–1737.

[36] G. Thompson, M. Miller, H. Fraser, Some aspects of atom probe specimen preparation and analysis of thin film materials, Ultramicroscopy 100 (2004) 25–34.

[37] B. Gault, D. Haley, F. de Geuser, M. Moody, E. Marquis, D. Larson, B. Geiser, Advances in the reconstruction of atom probe tomography data, Ultramicroscopy 111 (2011) 448–457.

[38] L. T. Stephenson, A. V. Ceguerra, T. Li, T. Rojhirunsakool, S. Nag, R. Banerjee, J. M. Cairney, S. P. Ringer, Point-by-point compositional analysis for atom probe tomography, MethodsX 1 (2014) 12–18.

[39] A. Woodfield, P. Postans, M. Loretto, R. Smallman, The effect of long-term high temperature exposure on the structure and properties of the titanium alloy Ti 5331S, Acta Metallurgica 3 (1998) 507–515.

[40] C. Ramachandra, V. Singh, Silicide precipitation in alloy Ti-6AI-5Zr-0.5Mo-0.25Si, Metallurgical Transactions A 13 (1982) 771–775.

[41] J. Okamoto, C. Ahn, B. Fultz, Short range ordering in face centered cubic Ni_3Al, Journal of Applied Physics 77 (1995) 4380–4383.

[42] C. Ramachandra, V. Singh, Effect of silicide precipitation on the low cycle fatigue behaviour of alloy Ti-6.3Al-2Zr-3.3Mo-O.3OSi, Scripta Metallurgica 21 (1987) 633–636.

[43] L. Lenssen, FIM/atom probe study of titanium alloy, Master's thesis, Department of Materials, University of Oxford, 1987.

List of Tables

Table 1: Ti-alloy heat treatments as investigated by TEM and APT. Qualitative assessment of reflection visibility (SADP), the visibility of precipitates in dark field (DF) and the observation of ordered clusters using APT are summarised. In addition, the number of ions run in each APT needle is provided.

[°C]/days	SADP	DF	APT 50NN	No. ions (m)
Ti-7Al				
IWQ	not visible	no	none	20, 8
AC	not visible	no	none	20, 42
625/14	very very weak	no	none	44, 7, 6, 8, 60
550/28	very weak	no	none	12, 11, 27, 18
550/84	weak	20×150 nm	none	16
Ti-6Al-4V				
SC	weak	no		
625/14	strong	no	barely	6, 8, 14, 5, 8, 15
550/28	strong	variations	ordered regions	13, 3

Table 2: Overall composition of the Ti-7Al needles examined, in wt. and at.%. Trace levels of H, N and C were also present.

	Al		O	
Sample	wt.%	at.%	wt.%	at.%
IWQ	6.8	11.5	0.4	1.1
AC	6.5	10.9	0.2	0.6
625/14	6.3	10.6	0.2	0.6
550/28	6.9	11.6	0.2	0.6
550/84	4.1	7.0	0.3	0.8

List of Figures

a) b)

Figure 1: Ti-7Al ingots were a) β forged and b) hot rolled.

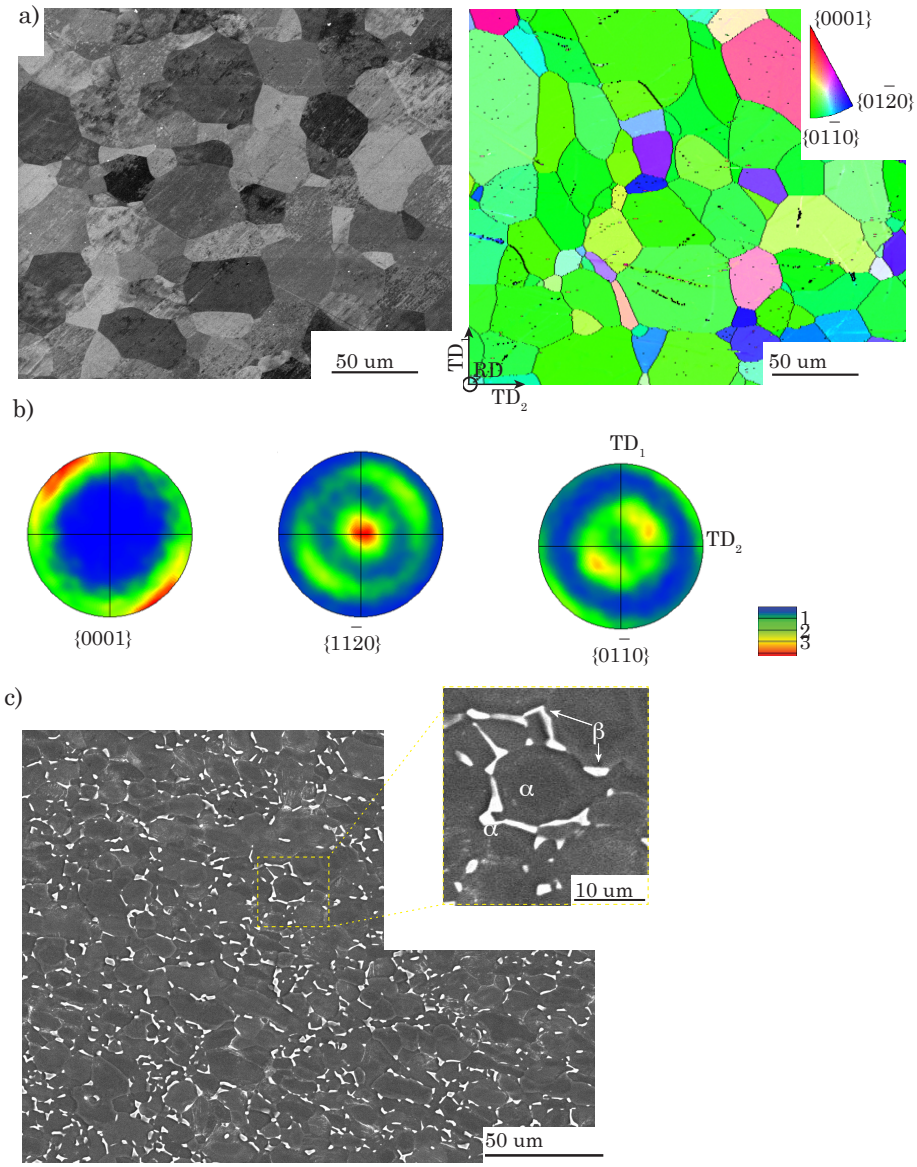

Figure 2: a) Microstructure in the Ti-7Al bar (left, BSEM and right, EBSD). The transverse directions (TD_1 and TD_2) and rolling direction (RD) of the bar are marked. b) Texture pole figure from an area of 2500×2000 μm, ~ 4000 grains. c) BSEM micrograph of Ti-6Al-4V microstructure; equiaxed α grains and platelets of β between α.

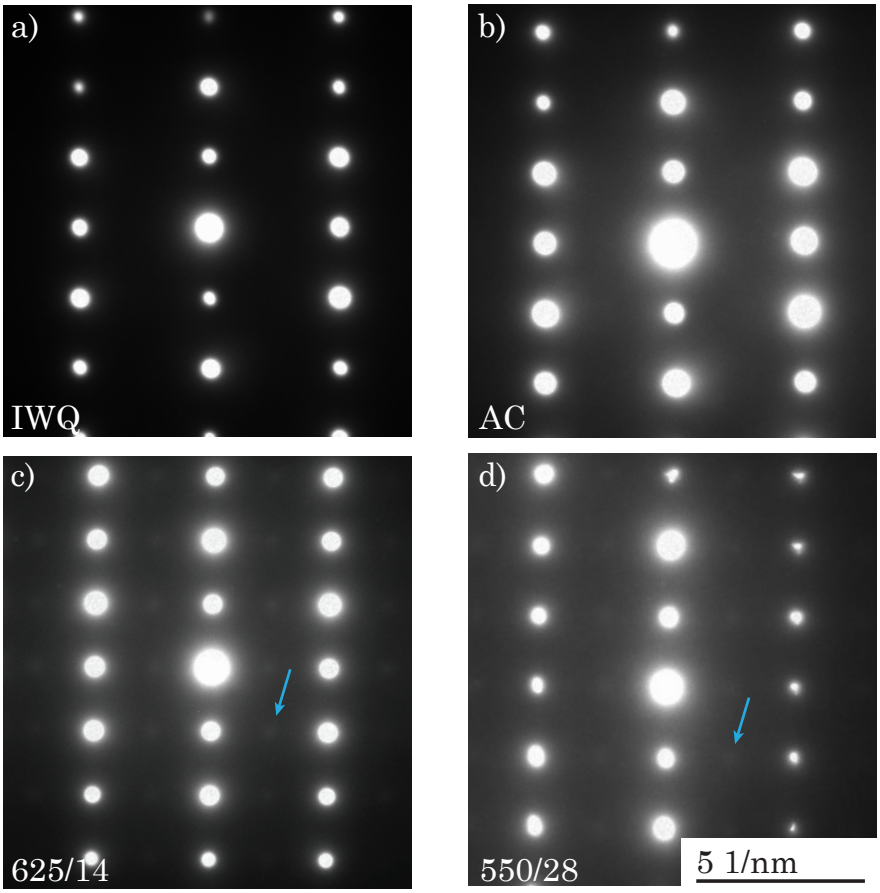

Figure 3: Ti-7Al, selected area [$2\bar{1}\bar{1}0$] diffraction patterns in the a) IWQ), b) AC, c) 625/14 and d) 550/28. The superlattice reflections are marked by arrows.

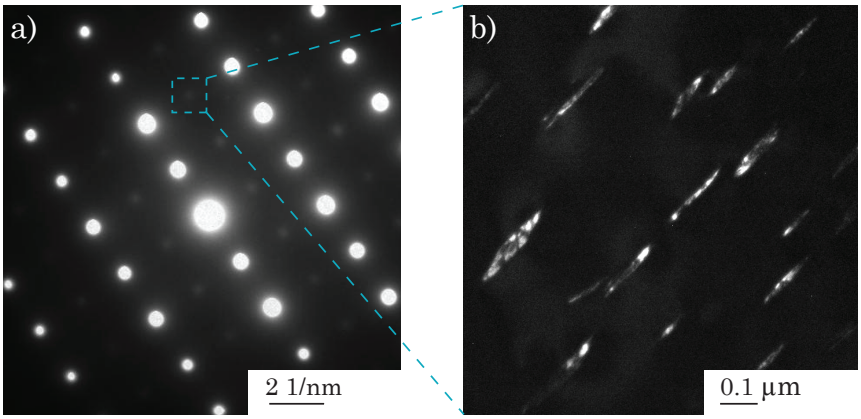

Figure 4: a) Selected area [$2\bar{1}\bar{1}0$] diffraction pattern of Ti-7Al after heat treating at 550°C for 84 days. b) Dark-field image of the ordered regions in Ti-7Al (550/84), taken from the marked superlattice spot.

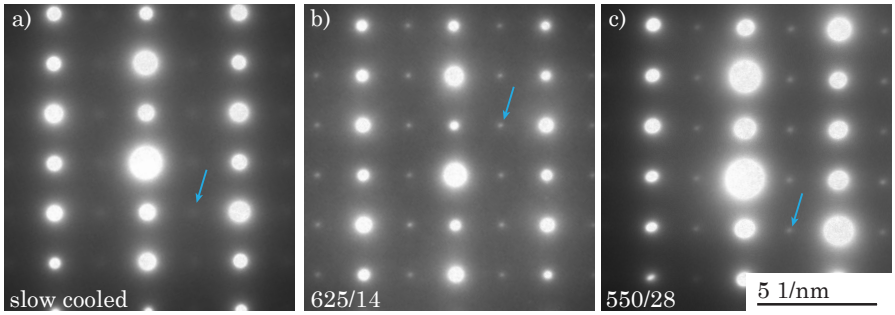

Figure 5: Ti-6Al-4V, selected area $[2\bar{1}\bar{1}0]$ diffraction patterns in the a) SC, b) 625/14, c) 550/28. The superlattice reflections are marked by arrows.

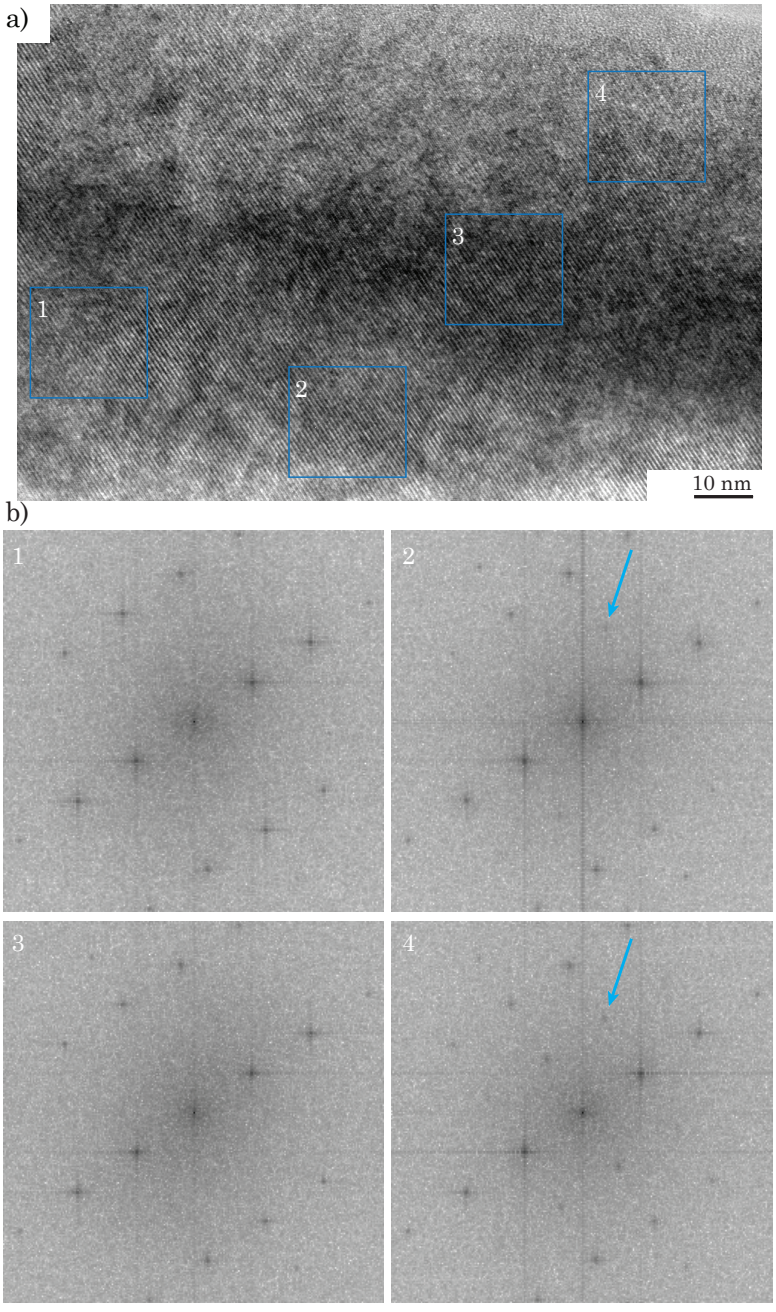

Figure 6: a) Phase contrast HRTEM lattice image of the ordered regions in Ti-6Al-4V (550/28). b) Series of $[2\bar{1}\bar{1}0]$ FFT pesudo-diffraction patterns processed from boxes marked 1-4. The intensity scale has been inverted to highlight the superlattice reflections (marked by arrows).

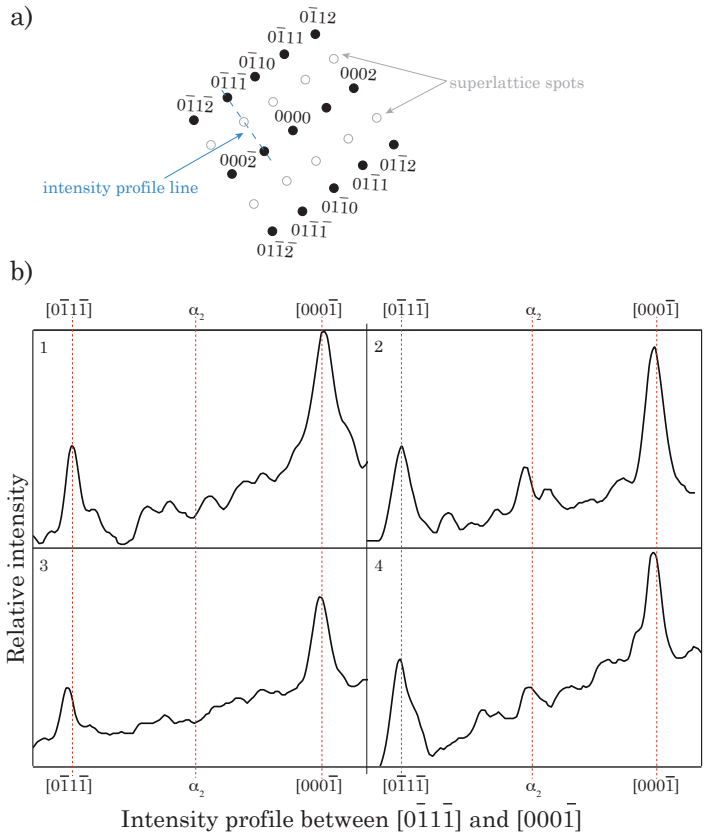

Figure 7: a) Simulated $[2\bar{1}\bar{1}0]$ diffraction pattern. b) Intensity profiles between the two diffraction spots marked by a blue line on (a), for the locations (1-4) in the Ti-6Al-4V 550/28 sample in Figure 6, using the FFT pseudo-diffraction patterns obtained. A Gaussian filter was applied to the FFT patterns.

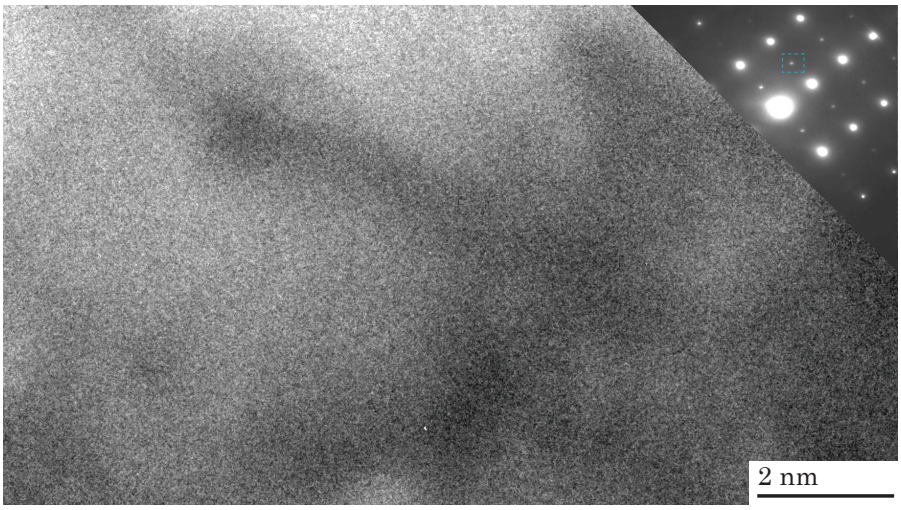

Figure 8: Dark field TEM image taken using the superlattice spot in the Ti-6Al-4V 550/28 sample, using a Titan image corrected TEM.

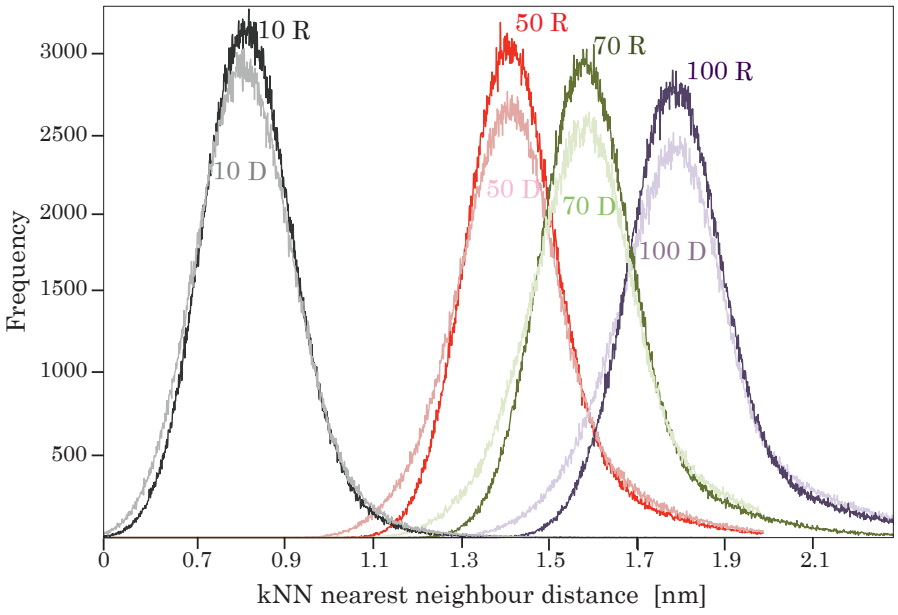

Figure 9: Distribution of first kNN neighbour distances for a Ti-6Al-4V (550/28) random solid solution (R) in comparison with the collected data (D).

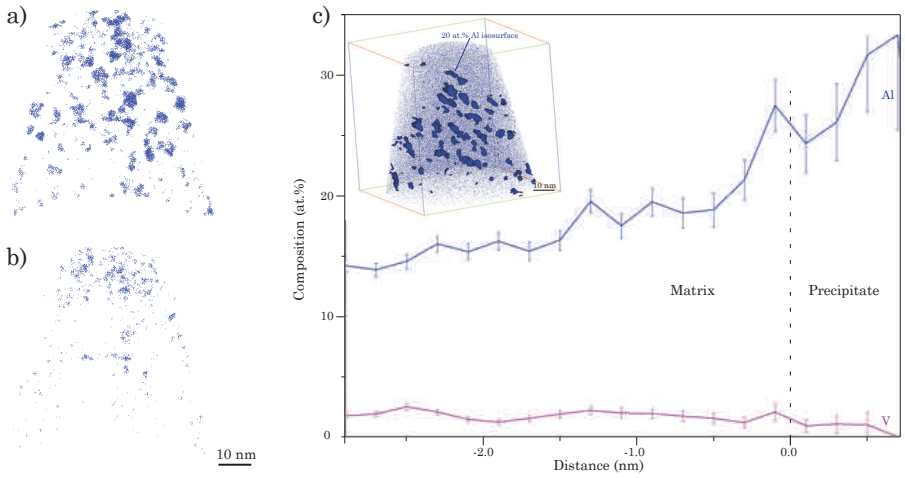

Figure 10: Using the 50NN analysis the high-density Al regions of the data have been highlighted in the atom maps a) experimental data b) randomised system. c) Aluminium concentration profile measured across interfaces averaged over five similar features identified by the 20 at.% Al iso-concentration surface.